Long-range ordering of turbulent stresses in two-dimensional flow

Yang Liao and Nicholas T. Ouellette

Phys. Rev. E **91**, 063004 — Published 12 June 2015

DOI: 10.1103/PhysRevE.91.063004

Long-range ordering of turbulent stresses in two-dimensional flow

Yang Liao and Nicholas T. Ouellette*
Department of Mechanical Engineering & Materials Science, Yale University, New Haven, CT 06520, USA

Using filter-space techniques, we study the spatial structure of the turbulent stress that couples motion on different length scales in a quasi-two-dimensional laboratory flow. As the length scale increases, we observe the appearance of long-range, system-spanning spatial order of this stress, even though the flow field remains disordered. Suggestively, this ordering occurs only in the range of scales over which we find net inverse energy transfer to larger scales. However, we find that a field built from wavevectors with random phases also displays ordering, suggesting that at least some of the ordering we observe is purely kinematic. Our results help to clarify the role played by geometric alignment in the turbulent energy cascade, and highlight the importance of the scale-dependent rate of strain in the energy transfer process.

PACS numbers: 47.27.-i, 05.65.+b, 89.75.Fb

I. INTRODUCTION

Turbulent flows are highly unsteady, chaotic, and characterized by dynamics occurring on a vast range of length and time scales, but they are not random. In many cases, including the generation of large-scale circulation in turbulent convection [1] or a net magnetic field in a turbulent dynamo [2], the violent fluctuations [3, 4] that make turbulence difficult to model can produce surprising order. Intense turbulence also tends to *self*-organize: the classical Richardson–Kolmogorov energy cascade [5, 6], for example, requires a delicate internal balance of the interactions between different scales of motion. However, determining the precise mechanisms by which turbulence produces such order, both of transported quantities and of its internal dynamics, remains a challenge.

Fundamentally, it is the nonlinear term in the Navier–Stokes equations that couples dynamics on different length scales via wavevector triad interactions, allowing the transfer of energy and momentum between scales. In principle, all scales are coupled; but in practice, the net effect of these nonlinear effects in three-dimensional turbulence is to drive a scale-to-scale cascade of energy from large length scales where it is injected into the flow to small scales where it is dissipated into heat by the action of molecular viscosity [5, 6]. This directed energy flow imposes restrictions on the nonlinear interactions allowed in turbulence, since not all types of triads drive energy to small scales [7]. Understanding why some scale couplings are promoted while others are suppressed would make it easier to devise accurate but simplified turbulence models for practical engineering applications.

The net action of these triads can be expressed via a scale-dependent turbulent stress tensor; the inner product of this stress and the scale-resolved rate of strain determines the local energy flux between scales of motion. Due to this inner product, the relative alignment of the eigenframes of the stress and the rate of strain determines the direction of the energy flux (that is, from large to small scales or vice versa); additionally, the local energy flux can be suppressed entirely due to misalignment of these eigenframes. Thus, the spatial organization of the turbulent stress and the scale-resolved rate of strain contains information about the directionality and strength of the energy cascade [8].

Here, we study the alignment of these turbulent stress and strain rates in a quasi-two-dimensional laboratory flow using filter-space techniques. We show that for scales in the regime where we observe net transfer of energy to large scales (consistent with the celebrated inverse energy cascade of two-dimensional turbulence), the turbulent stress displays long-range spatial order: its eigenframe aligns across the entire system, which we quantify with an appropriate order parameter. However, we also show that a synthetic velocity field built from Fourier modes with random phases shows very similar behavior, implying that at least some of what we observe is purely kinematic. Our results add to the current understanding of the role of geometric alignment in the physics of the energy cascade, and raise several intriguing possibilities and questions for future study.

We begin below by briefly describing our experimental and analysis methods in Sec. II. Our results are described in Sec. III, beginning with a discussion of the mean-field behavior we observe in our experiment, followed by a demonstration of the alignment transition we see in the turbulent stress. We then describe our tests using random Fourier modes. Finally, in Sec. IV, we discuss some of the implications of our results and outline some directions for future study.

II. METHODS

A. Experiment

To study the properties of the scale-to-scale energy transfer and the turbulent stresses that drive it, we used a quasi-two-dimensional laboratory flow that can be driven

* nicholas.ouellette@yale.edu

into (weak) turbulence. Our experimental apparatus is described in detail elsewhere [9–11]; briefly, we generated quasi-two-dimensional flow by placing a thin layer (5 mm deep) of NaCl dissolved in water (16% by mass) above a grid of neodymium-iron-boron permanent magnets arranged in stripes of alternating polarity. When a dc electric current (here, 1.25 A) is driven laterally through the fluid layer, Lorentz forces set the fluid into motion [9, 10, 12–15]. The total size of the driven area is 86 cm × 86 cm (= $34L_m \times 34L_m$, where L_m is the center-to-center magnet spacing), of which we measure the central 32 cm × 23 cm region (= $12L_m \times 9L_m$). For the data here, the Reynolds number based on the root-mean-square velocity and L_m is Re = 270. Note that, when defined in this way, the Reynolds number is essentially a non-dimensionalization of the electric current [16], rather than encoding the scale separation as a true turbulent Reynolds number would.

To measure the flow, we use particle tracking velocimetry. Polystyrene tracer particles of diameter 51μm are suspended at the interface between the salt-water layer and a second, less dense layer of pure water (also 5 mm deep). We image the particles with a 4 megapixel camera at 60 frames per second, and follow their motion with a predictive tracking algorithm [17]. Instantaneous velocities are computed from the particle trajectories by convolving them with a Gaussian smoothing and differentiating kernel [18]. We image ∼30,000 particles per frame with an average separation of 0.8 mm, allowing us to measure time-resolved velocity fields [9]. To construct velocity fields from the particle data, we use the particle positions in each frame to create a triangulated mesh to which we can apply finite-element tools to calculate spatial gradients. We project the velocity fields onto a basis of streamfunction eigenmodes to remove any three-dimensional effects [9], resulting in a loss of less than 4% of the kinetic energy [10].

B. Filter-Space Techniques

The precise details of the energy cascade are difficult to access directly. Energy transfer between scales can formally be written as the interaction of triads of modes in Fourier space [19], but such wavevector interactions cannot be localized in space. Thus, one can typically study turbulence as a function of scale or space but not both. Recently, however, an approach based on low-pass filtering of the equations of motion has allowed the measurement of the energy flowing between scales at every point in space and time [20–22]. This powerful new technique has been particularly useful in providing insight into the mechanisms that drive two-dimensional turbulence [12, 23–27]. In this filtering formalism, the spectral energy flux between scales can be written as

$$\Pi^{(L)} = -\left[(u_i u_j)^{(L)} - u_i^{(L)} u_j^{(L)}\right] \frac{\partial u_i^{(L)}}{\partial x_j} = -\tau_{ij}^{(L)} s_{ij}^{(L)}, \tag{1}$$

where u_i is the i^{th} component of the velocity and summation is implied over repeated indices. The superscript (L) denotes a quantity low-pass filtered at a scale L, so that variation on spatial scales finer than L is suppressed. $s_{ij}^{(L)}$ is the filtered rate-of-strain tensor (the symmetric part of the velocity gradient), and is analogous to the rate of strain of the full velocity field. But the tensor $\tau_{ij}^{(L)} = (u_i u_j)^{(L)} - u_i^{(L)} u_j^{(L)}$ has no analog in the full equations of motion, and arises as a direct consequence of the nonlinearities. Note that no assumptions of fully developed turbulence or self-similar scaling have been made in this definition, and that extremely fine spatial resolution is not required to use it on real data [28]. $\tau_{ij}^{(L)}$ plays the role of a stress tensor (similar to the Reynolds stress in the Reynolds-averaged Navier–Stokes equations [19]), and encodes the momentum coupling between the scales smaller than L and those that are larger. Equation (1) can be interpreted as expressing the rate of work done by the large-scale strain against stresses arising from the small-scale motion. With our sign convention, $\Pi^{(L)} > 0$ means that energy is being transferred to smaller scales, while $\Pi^{(L)} < 0$ means that energy is flowing to larger scales.

Experimentally, we remove the small-scale component of our measured velocity fields by convolving them with a function that acts as a low-pass filter in Fourier space. Our results are not very sensitive to the precise filter shape. Here, we used a spatially isotropic finite impulse response filter designed by convolving a sharp spectral filter with a frequency cutoff of $2\pi/L$ with a Gaussian window function to reduce ringing.

III. RESULTS

A. Mean-Field Results

Figure 1(a) shows our measurements of $\Pi^{(L)}$ averaged over space and time. As has been reported previously [12, 23, 25], for scales somewhat larger than L_m, $\Pi^{(L)} < 0$ and energy flows primarily to larger scales in accordance with the standard Kraichnan–Leith–Batchelor inverse-cascade phenomenology [15, 29–31]. We do not observe a range of constant energy flux, since our Reynolds number is relatively low and direct dissipation by viscosity and friction may play a role at all scales [32]. Figure 1(a) does, however, unambiguously show net inverse energy transfer. To probe this behavior in more detail, we first note that eq. (1) is an inner product. Thus, it is sensitive to the relative alignment between $\tau_{ij}^{(L)}$ and $s_{ij}^{(L)}$, and misalignment of these two tensors can suppress the energy transfer.

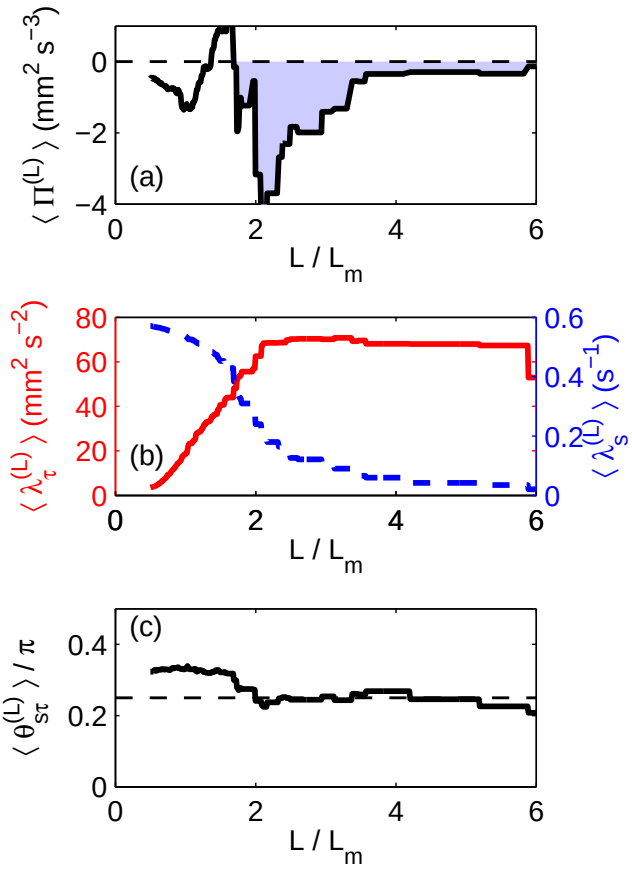

FIG. 1. (color online) (a) Spatially averaged spectral energy flux computed from eq. (4) as a function of filter scale L/L_m, where L_m is the magnet spacing. Negative values denote transfer to larger scales; the shaded region shows the inverse energy cascade. (b) Spatially averaged eigenvalues of $\tau_{ij}^{(L)}$ ($\langle\lambda_\tau^{(L)}\rangle$; solid line; left axis) and $s_{ij}^{(L)}$ ($\langle\lambda_s^{(L)}\rangle$; dashed line; right axis) as a function of L/L_m. (c) Spatially averaged angle $\langle\theta_{s\tau}\rangle$ between the eigenframes of $\tau_{ij}^{(L)}$ and $s_{ij}^{(L)}$ as a function of L/L_m. The dashed line shows $\pi/4$.

To see this effect more clearly, we first note that $\tau_{ij}^{(L)}$ and $s_{ij}^{(L)}$ are symmetric, two-dimensional tensors. Incompressibility requires that the trace of $s_{ij}^{(L)}$ vanish, so that $s_{ii}^{(L)} = 0$; this restriction also implies that it is only the traceless (deviatoric) part of the stress that gives a nonzero contribution to $\Pi^{(L)}$. Denoting the deviatoric part of the stress as $\mathring{\tau}_{ij}^{(L)}$, we can write

$$\Pi^{(L)} = -\left(\mathring{\tau}_{ij}^{(L)} + \frac{1}{2}\tau_{kk}\delta_{ij}\right) s_{ij}^{(L)} = -\mathring{\tau}_{ij}^{(L)} s_{ij}^{(L)}, \qquad (2)$$

where δ_{ij} is the identity tensor. Since this equation is the trace of the matrix product of $\mathring{\tau}_{ij}^{(L)}$ and $s_{ij}^{(L)}$, it is basis independent. Working in the eigenbasis of $\mathring{\tau}_{ij}^{(L)}$, we can write

$$\Pi^{(L)} = -\,\mathrm{Tr}\left[\begin{pmatrix}\lambda_\tau^{(L)} & \\ & -\lambda_\tau^{(L)}\end{pmatrix}\begin{pmatrix}\cos\theta_{s\tau}^{(L)} & -\sin\theta_{s\tau}^{(L)} \\ \sin\theta_{s\tau}^{(L)} & \cos\theta_{s\tau}^{(L)}\end{pmatrix} \begin{pmatrix}\lambda_s^{(L)} & \\ & -\lambda_s^{(L)}\end{pmatrix}\begin{pmatrix}\cos\theta_{s\tau}^{(L)} & \sin\theta_{s\tau}^{(L)} \\ -\sin\theta_{s\tau}^{(L)} & \cos\theta_{s\tau}^{(L)}\end{pmatrix}\right], \qquad (3)$$

where $\lambda_\tau^{(L)}$ and $\lambda_s^{(L)}$ are the eigenvalues of $\mathring{\tau}_{ij}^{(L)}$ and $s_{ij}^{(L)}$, respectively, and $\theta_{s\tau}^{(L)}$ is the angle between the two eigenframes. Multiplying these matrices, we arrive at [26]

$$\Pi^{(L)} = -2\lambda_\tau^{(L)}\lambda_s^{(L)}\cos 2\theta_{s\tau}^{(L)}. \qquad (4)$$

In Fig. 1(b), we plot the spatially averaged eigenvalues, which both rapidly reach scale-independent values in the inverse-cascade range. Figure 1(c) shows the average of $\theta_{s\tau}^{(L)}$; as reported previously [25], it is nearly constant and equal to $\pi/4$ throughout the inverse cascade, suggesting that the mean-field behavior of the inverse cascade can be captured by a tensor eddy viscosity that imposes a 45° rotation between $\tau_{ij}^{(L)}$ and $s_{ij}^{(L)}$, even though $\Pi^{(L)}$ vanishes for $\theta_{s\tau}^{(L)} = \pi/4$. But Fig. 1 also makes it clear that a simple mean-field model cannot capture all of the relevant physics: the mean spectral energy flux shown in Fig. 1(a) is not constant over the inverse cascade range, even though the individual mean values of $\lambda_\tau^{(L)}$, $\lambda_s^{(L)}$, and $\theta_{s\tau}^{(L)}$ vary little in this range. The structure of $\langle\Pi^{(L)}\rangle$ is not captured by the variation in $\langle\lambda_\tau^{(L)}\rangle$, $\langle\lambda_s^{(L)}\rangle$, and $\langle\theta_{s\tau}^{(L)}\rangle$.

B. Local Structure and Stress Ordering

To move past a mean-field description, we take advantage of the true power of filter-space techniques and consider the spatial distribution of the components that contribute to the spectral energy flux. In particular, we are interested in the orientation of the eigenframes of $\tau_{ij}^{(L)}$ and $s_{ij}^{(L)}$: as is evident from eq. (4), misalignment of these eigenframes can suppress the spectral energy flux even if the eigenvalues are large. To illustrate this effect, in Fig. 2 we show the spatially resolved energy flux along with the contours where $\theta_{s\tau}^{(L)} = \pi/4$ and $3\pi/4$ as well as spatial maps of $\lambda_\tau^{(L)}$ and $\lambda_s^{(L)}$ for the same instant in time for a filter scale of $L = 3L_m$. The eigenvalue fields are not obviously related to the spectral flux, but the given contours of $\theta_{s\tau}^{(L)}$ lie perfectly on the contours of vanishing energy flux. We note that in some cases the $\pi/4$ and $3\pi/4$ contours of $\theta_{s\tau}^{(L)}$ lie nearly on top of each other; we do not currently understand the precise meaning of this behavior.

Nevertheless, it is clear that the alignment of the eigenframes of the turbulent stress and the resolved strain rate

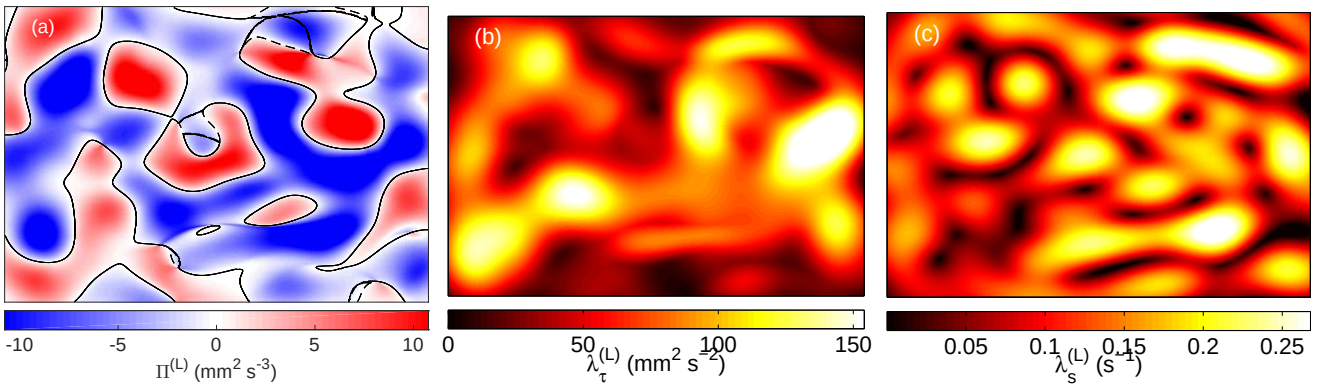

FIG. 2. (color online) (a) Spatial map of the spectral energy flux $\Pi^{(L)}$ computed for a filter scale of $L = 3L_m$. The black contours show the places where $\theta_{s\tau}^{(L)} = \pi/4$ (solid black lines) and $3\pi/4$ (dashed black lines). (b,c) The eigenvalues of (b) the stress $\lambda_\tau^{(L)}$ and (c) the strain rate $\lambda_s^{(L)}$ computed for the same instant of time and the same filter scale.

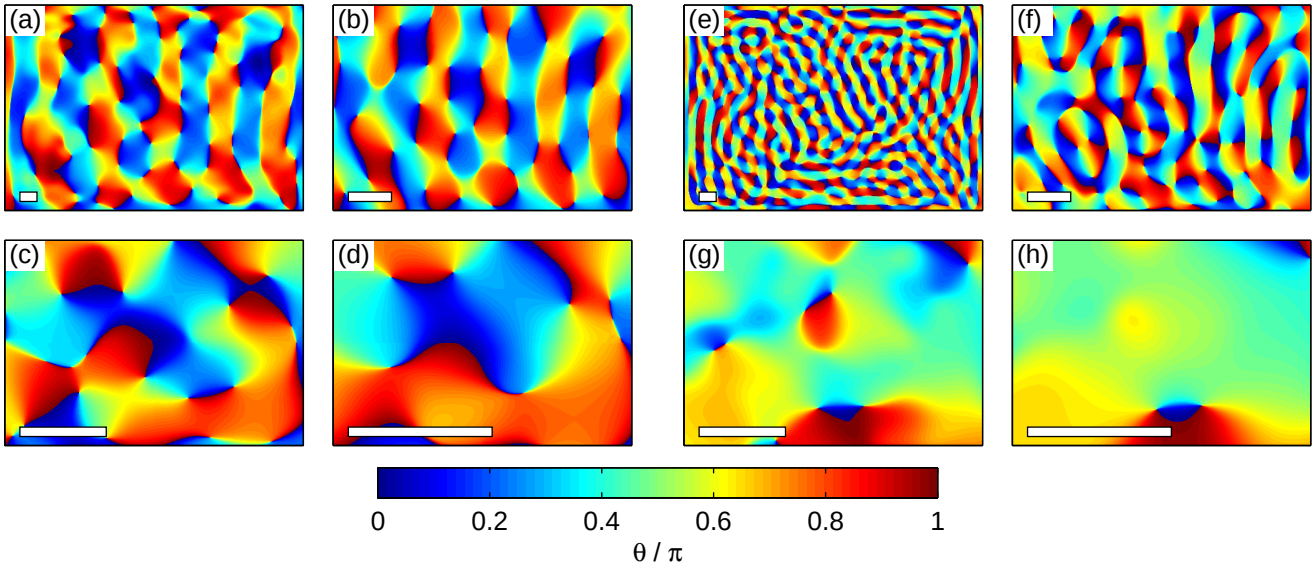

FIG. 3. (color online) Spatially resolved orientation of the local (a-d) $s_{ij}^{(L)}$ and (e-h) $\tau_{ij}^{(L)}$ eigenframes at a single time. The color shows the angle between the largest eigenvector and the horizontal axis, in units of π. Data are shown for four filter scales L, shown by the scale bars: (a,e) $0.6L_m$, (b,f) $1.5L_m$, (c,g) $3L_m$, and (d,h) $5L_m$. As L increases, the patterns for both tensors coarsen; but the stress aligns over nearly the entire system at large L, while the strain rate does not.

appears to dominate the spatial distribution of the spectral energy flux. To study it in further detail, in Fig. 3(a-d) we plot the orientation θ (relative to a fixed horizontal axis) of the largest eigenvector of $s_{ij}^{(L)}$ at four different filter scales L. As L grows and small-scale variation is removed, the spatial pattern of orientation coarsens, as it must. The situation, however, is markedly different for $\tau_{ij}^{(L)}$ (Fig. 3(e-h)). For small L, the spatial variation in the orientation of $\tau_{ij}^{(L)}$ is much more rapid than for $s_{ij}^{(L)}$ (Fig. 3(a,e)). But for larger L, the variation is much *slower*: $\tau_{ij}^{(L)}$ appears to be aligning across nearly the entire system. Suggestively, this slow variation occurs in the range of scales where we see net inverse energy transfer (Fig. 3(d,h)). Although data are shown here for only a single Reynolds number, we see similar alignment as a function of scale for all Reynolds numbers where we observe net inverse energy transfer. This alignment therefore does not appear to be associated with the transition to turbulence.

We can quantify this alignment with an appropriate order parameter. Noting that eigenvectors are essentially apolar (since an eigenvector rotated by 180° is the same eigenvector), we compute a scalar order parameter used to study nematic ordering in two-dimensional liquid crys-

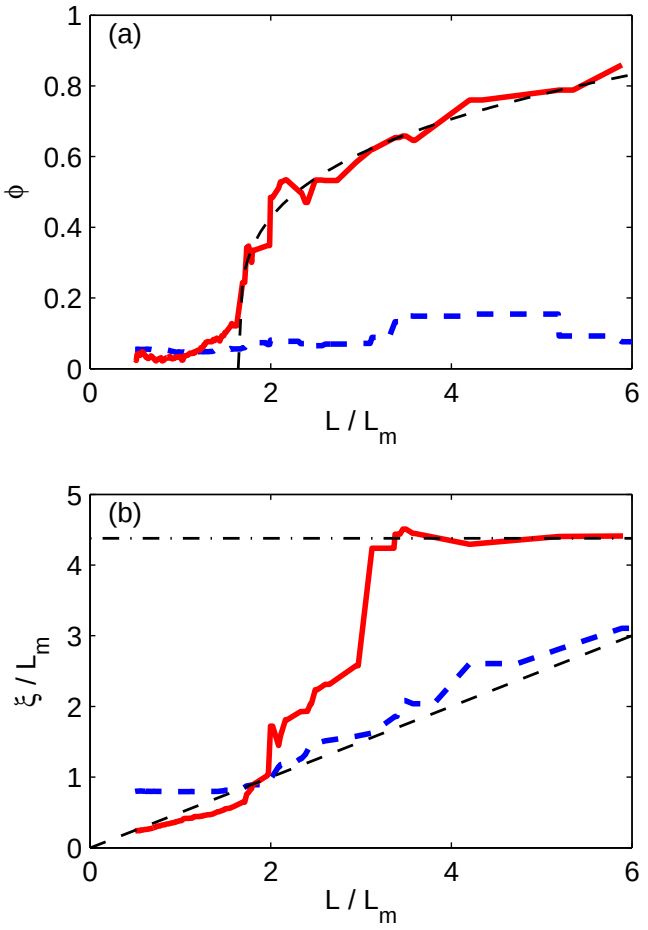

FIG. 4. (color online) (a) The order parameter ϕ for $\tau_{ij}^{(L)}$ (solid line) and $s_{ij}^{(L)}$ (thick dashed line) as a function of L/L_m. Beginning at an onset length scale $L_c = 1.64L_m$, $\tau_{ij}^{(L)}$ rapidly orders in space, while $s_{ij}^{(L)}$ does not. The thin dashed line is a power-law fit to the data, with an exponent of 0.27 ± 0.02. (b) Correlation length ξ of the orientation fluctuations for $\tau_{ij}^{(L)}$ (solid line) and $s_{ij}^{(L)}$ (thick dashed line). The thin dashed line shows the expected correlation lengths for a field that coarsens only due to the filtering; the thin dot-dashed line is the largest ξ can be given our finite experimental domain. The observed plateau in ξ for $\tau_{ij}^{(L)}$ at large L/L_m is a finite-domain effect.

tals. We plot this order parameter, defined as [33, 34]

$$\phi = 2\sqrt{\left(\langle\cos^2\theta\rangle - \frac{1}{2}\right)^2 + \langle\cos\theta\sin\theta\rangle^2}, \qquad (5)$$

where the averages are taken over space, as a function of L for both $\tau_{ij}^{(L)}$ and $s_{ij}^{(L)}$ in Fig. 4(a). The orientation patterns for $s_{ij}^{(L)}$ coarsen with increasing L, but ϕ remains low and $s_{ij}^{(L)}$ shows no long-range orientational order. For small L, the situation is similar for $\tau_{ij}^{(L)}$. But at a particular scale that nearly coincides with the onset of net inverse energy transfer (see Fig. 1(a)), ϕ grows rapidly for $\tau_{ij}^{(L)}$ and approaches unity for large L. The growth of ϕ with L roughly follows a power law; fitting a function of the form $\phi \sim (L - L_c)^n$)to the data, we obtain an onset scale of $L_c = 1.64L_m$ and an exponent of $n = 0.27 \pm 0.02$.

We also measured the correlation length ξ of the orientation fluctuations. We computed the spatial correlation functions of the orientation fluctuations of the eigenvectors of $\tau_{ij}^{(L)}$ and $s_{ij}^{(L)}$. Specifically, suppose $\mathbf{e}(\mathbf{x})$ is an eigenvector of one of these tensors. Its spatial fluctuations are given by $\mathbf{e}(\mathbf{x})' \equiv \mathbf{e}(\mathbf{x}) - \langle\mathbf{e}(\mathbf{x})\rangle$, where the angle brackets denote an average taken over space at a single time. We define the correlation function as

$$C(r) = \frac{\langle \mathbf{e}(\mathbf{x})' \cdot \mathbf{e}(\mathbf{x}+\mathbf{r})'\rangle}{\langle \mathbf{e}(\mathbf{x})' \cdot \mathbf{e}(\mathbf{x})'\rangle}, \qquad (6)$$

where r is the magnitude of $\mathbf{r}$. Since these fluctuations are measured relative to the mean orientation across the measurement domain and the orientation field is not uniform, $C(r)$ must cross zero at some r. We estimate the correlation length ξ to be the first zero crossing of $C(r)$. The results are plotted in Fig. 4(b). For $s_{ij}^{(L)}$, ξ increases as expected given our filtering (as we remove small-scale variation, ξ must grow at least as fast as $L/2$). But at L_c, ξ computed for $\tau_{ij}^{(L)}$ begins to increase much more rapidly before saturating at the largest value allowed by the size of our measurement domain (equal to half of the diagonal distance across our measurement domain). Thus, our results so far suggest that net inverse energy flux is associated with long-range ordering of the turbulent stress that drives the spectral energy transfer. This ordering is distinct from simple coarsening of the flow field, as it differs from what we observe for the rate of strain.

However, there are also some indications that the ordering behavior we observe may not in fact be causally related to any turbulent dynamics. For example, even though we observe the appearance of long-range order as a function of *scale*, the flow itself is always in the same macroscopic state. The control parameter that governs the dynamical state of the system (the Reynolds number) does not control the appearance of order. Thus, to gain more insight into our empirical observations, we turn to a simple model system.

C. Ordering in a Random Field

As shown above, we observe long-range spatial ordering in the turbulent stress, but not in the filtered rate of strain. It is possible that this transition is due to the dynamics of turbulent energy transfer. However, the Reynolds number does not appear to affect the appearance of order; additionally, $\tau_{ij}^{(L)}$ and $s_{ij}^{(L)}$ are quite different in that $\tau_{ij}^{(L)}$ is quadratic in the velocity, while $s_{ij}^{(L)}$ is linear. Thus, there are hints that at least part of what we observe may in fact be independent of the turbulence.

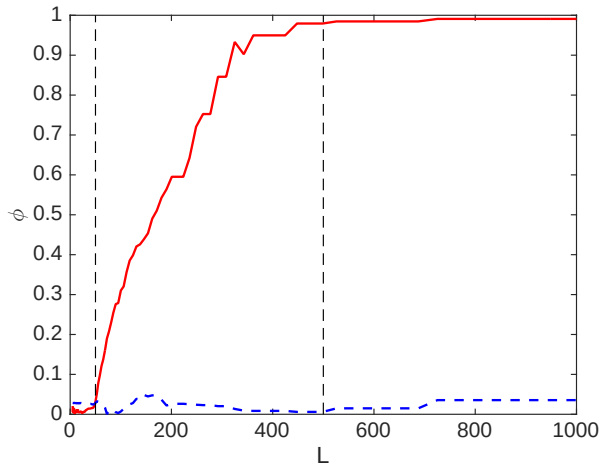

FIG. 5. (color online) The order parameter ϕ computed for $\tau_{ij}^{(L)}$ (solid line) and $s_{ij}^{(L)}$ for a random field. The parameters used to construct the field are given in the text. The vertical dashed lines show the size of the largest and smallest mode.

To explore the ordering in more detail, we used a simple model to build a random flow field. Taking an approach conceptually similar to kinematic simulation [35], although without any dynamics, we constructed an incompressible "velocity" field by summing over Fourier modes with random phases. Specifically, following Fung and Vassilicos [35], the velocity field was defined to be

$$\mathbf{u} = \sum_{n=1}^{N_k} \left[\mathbf{A}_n \cos \mathbf{k}_n \cdot \mathbf{x} + \mathbf{B}_n \sin \mathbf{k}_n \cdot \mathbf{x} \right], \tag{7}$$

where the coefficients

$$\mathbf{A}_n = A_n \left(\cos \varphi_n, \ -\sin \varphi_n \right) \tag{8}$$

and

$$\mathbf{B}_n = B_n \left(-\cos \varphi_n, \ \sin \varphi_n \right) \tag{9}$$

and the wavevector

$$\mathbf{k}_n = k_n \left(\sin \varphi_n, \ \cos \varphi_n \right) \tag{10}$$

guarantee incompressibility. The phases $\varphi_n \in [0, 2\pi]$ are random variables drawn from a uniform distribution and are uniform in space but uncorrelated from scale to scale. The magnitudes of each mode are related to an assumed form of the energy spectrum $E(k)$ as $A_n^2 = B_n^2 = E(k_n)\Delta k_n$, where Δk_n is the mode spacing. Typically, one assumes a power-law form for the spectrum, so that $E(k) \sim k^{-p}$.

In Fig. 5, we show the order parameter ϕ computed for the turbulent stress and the filtered strain rate for a single example of a random field. The overall behavior of ϕ is clearly very similar to what we observed in the experiment (Fig. 4(a)): the strain rate does not order, while the stress orders rapidly above some critical scale. In fact, when compared to the experimental case, the behavior of ϕ is sharper, in that ϕ is closer to zero for the strain rate and closer to unity for the stress. For this example, the random field was constructed from 100 modes on a grid of 1000×1000 spatial locations. The length scale of the largest and smallest modes were $\ell_{\max} = 500$ and $\ell_{\min} = 50$, respectively. We assumed a Kolmogorov spectrum between $\ell_{\max}$ and $\ell_{\min}$, so that $E(k) \sim k^{-5/3}$ in this range; outside this range, $E(k) = 0$. However, we have found that our results are insensitive to all of these parameters: we see the same qualitative behavior for different choices of the number of modes and the size of the spatial domain.

What does change the order-parameter curve, however, is the choice of $\ell_{\max}$ and $\ell_{\min}$. We indicate these scales by vertical dashed lines in Fig. 5. We find that the ordering of the stress begins at $\ell_{\min}$, and that ϕ nearly saturates to unity at $\ell_{\max}$. To study the systematic effect of changing the scale separation, we first fixed $\ell_{\min}$ and varied $\ell_{\max}$, and then fixed $\ell_{\max}$ and varied $\ell_{\min}$, all while holding the number of modes and the spatial resolution of the random field constant. The results are shown in Fig. 6. From the curves plotted here, it is clear that our observations are largely confirmed, particularly when there is a reasonable separation of scales. The ordering transition for the stress occurs in the range of scales from $\ell_{\min}$ to $\ell_{\max}$; below $\ell_{\min}$, the stress does not display long-range order, and above $\ell_{\max}$, it is perfectly ordered.

In addition to changing $\ell_{\max}$ and $\ell_{\min}$, we also fixed these two scales and varied the shape of the energy spectrum. Somewhat surprisingly, our results are relatively insensitive to the spectral shape. In addition to the $k^{-5/3}$ spectrum shown here, we also tried a spectrum that scaled as $k^{-5/3}$ for small wavenumbers and k^{-3} for large wavenumbers, as would be expected in classical two-dimensional turbulence. Changing the spectrum in this way, however, had a negligible effect on the order-parameter curve. Using a spectrum that scaled as $k^{+5/3}$, so that the small scales were much more energetic than the large scales, resulted in a more rapid ordering with L, although the qualitative behavior was similar. For very steep spectra that scaled as k^{-p} with $p \gtrsim 5$, however, the behavior of the order-parameter curve was similar to that seen in Fig. 6(b) for large $\ell_{\min}$, where the order-parameter curve displayed an inflection point between the onset and saturation of ordering. But regardless of the spectral shape, we always observed ordering that began at $L \approx \ell_{\min}$ and saturated as $L \to \ell_{\max}$.

D. Fluctuations in Ordering

The previous section establishes that the turbulent stress computed for a random velocity field with no net energy flux also displays ordering; thus, at least part of the ordering must be a purely kinematic effect. However, there are differences between the order parameter

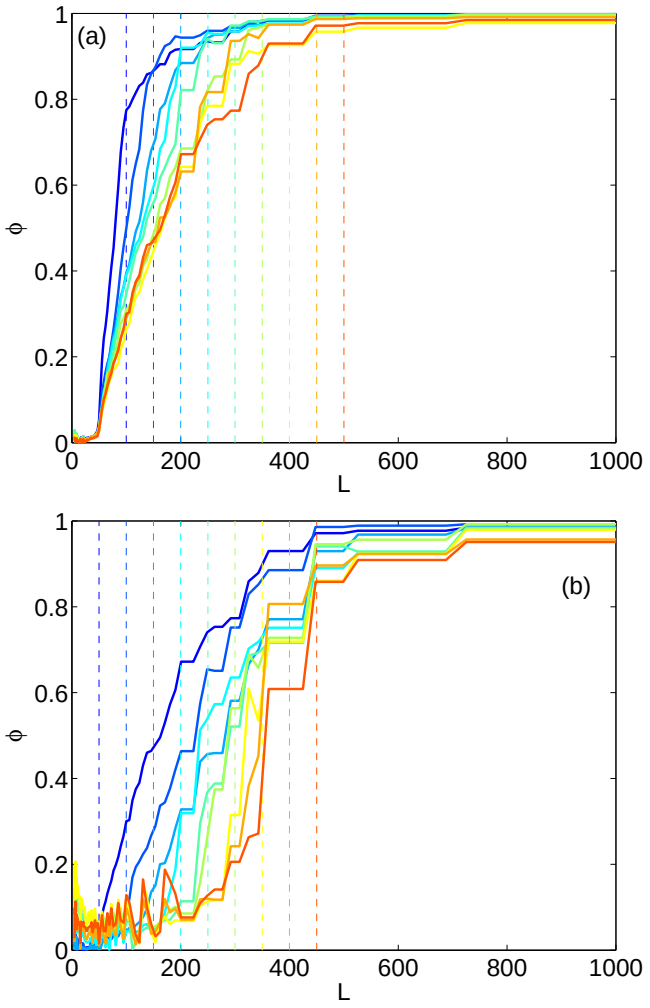

FIG. 6. (color online) The order parameter ϕ for the stress $\tau_{ij}^{(L)}$ computed for random velocity fields with varying $\ell_{\rm max}$ and $\ell_{\rm min}$. The fields were computed on a 1000×1000 grid with 100 modes, as in Fig. 5, and the mode amplitudes followed a $k^{-5/3}$ energy spectrum. (a) $\ell_{\rm min}$ was fixed at 50, and for the different solid curves $\ell_{\rm max}$ was varied in steps of 50 from 100 to 500. The different values of $\ell_{\rm max}$ are shown by the vertical dashed lines, and the color of these lines matches the corresponding order-parameter curves. (b) $\ell_{\rm max}$ was fixed at 500, and for the different solid curves $\ell_{\rm min}$ was varied in steps of 50 from 50 to 450. The vertical dashed lines show the values of $\ell_{\rm min}$.

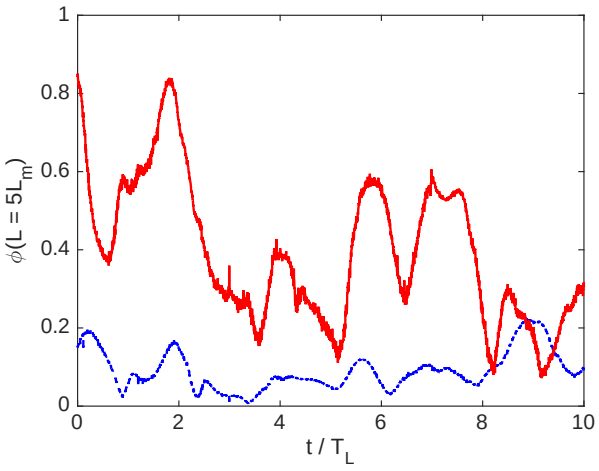

FIG. 7. (color online) The order parameter ϕ calculated from the experimental data for $L = 5L_m$ as a function of time (in units of T_L, the correlation time of the velocity field) for $\tau_{ij}^{(L)}$ (solid line) and $s_{ij}^{(L)}$ (lower dashed line). The fluctuations in the degree of order for the stress can be large, although the stress is nearly always more ordered than the strain rate.

curves for the experiment (Fig. 4(a)) and the random field (Fig. 5). In particular, ϕ always saturates to unity for the random field, while we never observe it reaching this asymptotic limit in the experiment. To probe this behavior, we consider a second distinction between the experiment and the random field: while the random field is a single snapshot, the experimental flow has rich time dynamics.

We focus on a fixed, large value of the filter scale L where we expect strong ordering; here, we choose $L = 5L_m$. In Fig. 7, we plot the time series of $\phi(L = 5L_m)$ for the experimental data. Strikingly, the degree of ordering of the turbulent stress we observe is not at all fixed in time, but rather fluctuates significantly, occasionally even falling below the degree of ordering for the filtered strain rate. This behavior is very different from what we see for an ensemble of random velocity fields, which exhibit only a small statistical scatter from instance to instance. This kind of large fluctuation mirrors what occurs in other turbulence-driven ordering phenomena: for example, the large-scale circulation in Rayleigh–Bénard convection undergoes reorientations and cessations [36], the magnetic field in a turbulent dynamo spontaneously flips [2], and the rotation sense of spectrally condensed flow in two-dimensional turbulence can reverse [37].

IV. DISCUSSION AND CONCLUSIONS

To summarize our results, we have shown that the turbulent stress $\tau_{ij}^{(L)}$ becomes more and more spatially ordered as the length scale L at which it is defined increases. Suggestively, this ordering takes place in the range of scales in our experimental flow over which we observe net inverse energy transfer. However, we see qualitatively similar ordering for a random synthetic velocity field with no coherent spectral dynamics. Thus, at least part of what we observe is kinematic, and likely arises from the quadratic dependence of the stress on the velocity field. This result is not necessarily negative; indeed, if one were to build a turbulence model incorporating the ordering we observe, its kinematic nature may be seen as a plus, as it is likely to hold in a wide range of flow conditions. But we also argue that part of the ordering is *not*

purely kinematic but depends on the turbulence, given that the alignment of the stress and the strain rate solely determines the directionality of the energy cascade (see eq. 4) and that the degree of order fluctuates strongly in time for the experimental flow.

Although fully teasing out the exact contributions of turbulence to the stress ordering is difficult, we can draw some conclusions from our results and make several conjectures that should be explored in further research. Regardless of the mechanism by which it does so, the stress certainly orders in space, meaning that the stress eigenvectors all point in the same direction. Since misalignment of the stress and strain rate can suppress the scale-to-scale energy flux (see Fig. 2) and the angle between the two controls the direction of the energy transfer, the net ordering of the stress suggests that what controls the energy cascade is in fact the orientation of the eigenframe of the strain rate. This result seems somewhat counterintuitive: the spectral energy transfer in turbulence arises from the mode coupling in the nonlinear term of the Navier–Stokes equations, and the turbulent stress, and not the strain rate, is a manifestation of this nonlinearity. However, it is what is suggested by the data.

Potentially more interesting is the observation from the random-field data that the ordering begins at the smallest length scale in the system and saturates at the largest scale. This result raises the possibility that characterizing the onset of ordering and the rate of the transition may be used as an instantaneous measure of the range of scales active in the turbulence. The idea of an inertial range delineated by a largest and smallest length scale is fundamental in our understanding of turbulence, but we typically only estimate these scales via mean-field arguments without being able to measure them instantaneously, particularly in experiments. Measuring the stress ordering may give us a way to access this information. We note that this conjecture suggests that the shape of the ordering transition should be a monotonic function of a turbulent Reynolds number that is based on the scale separation, a hypothesis that is directly testable in numerical simulation.

And finally, let us again note that we never observe perfect ordering of the stress in the experiment, and that the fluctuations of the degree of order in time are the feature that is the most different between the experimental results and the random field. It is possible that we do not observe perfect order because our measurement area is not large enough; but it is also possible that it is in fact the *lack* of perfect order that encodes the turbulence dynamics.

We hope that these results and conjectures will spur further work on the geometric structure of the energy cascade in turbulence. It also remains to be seen whether our results are peculiar to two-dimensional flows (where turbulent kinetic energy tends to Bose–Einstein condense into the lowest mode allowed in the system [14, 15, 29, 37]), or whether they can be extended to the three-dimensional case, where one would need to define a somewhat more complicated tensor order parameter. It will also be interesting to study the geometric dynamics of other manifestations of the nonlinearity in the Navier–Stokes equations, such as the analogous "vorticity stress" that drives the direct enstrophy cascade in two-dimensional turbulence.

ACKNOWLEDGMENTS

This work was supported by the U.S. National Science Foundation under grant DMR-1206399. We appreciate helpful discussions about this work with R. Ecke and H. Aluie.

[1] R. Krishnamurti and L. N. Howard, "Large-scale flow generation in turbulence convection," Proc. Natl. Acad. Sci. USA **78**, 1981–1985 (1981).

[2] M. Berhanu *et al.*, "Magnetic field reversals in an experimental turbulent dynamo," Europhys. Lett. **77**, 59001 (2007).

[3] B. I. Shraiman and E. D. Siggia, "Scalar turbulence," Nature **405**, 639–646 (2000).

[4] A. La Porta, G. A. Voth, A. M. Crawford, J. Alexander, and E. Bodenschatz, "Fluid particle accelerations in fully developed turbulence," Nature **409**, 1017–1019 (2001).

[5] L. F. Richardson, *Weather Prediction by Numerical Process* (Cambridge University Press, Cambridge, 1922).

[6] A. N. Kolmogorov, "The local structure of turbulence in incompressible viscous fluid for very large Reynolds numbers," Dokl. Akad. Nauk SSSR **30**, 301–305 (1941).

[7] L. Biferale, S. Musacchio, and F. Toschi, "Inverse energy cascade in three-dimensional isotropic turbulence," Phys. Rev. Lett. **108**, 164501 (2012).

[8] V. Borue and S. A. Orszag, "Local energy flux and subgrid-scale statistics in three-dimensional turbulence," J. Fluid Mech. **366**, 1–31 (1998).

[9] D. H. Kelley and N. T. Ouellette, "Onset of three-dimensionality in electromagnetically forced thin-layer flows," Phys. Fluids **23**, 045103 (2011).

[10] Y. Liao, D. H. Kelley, and N. T. Ouellette, "Effects of forcing geometry on two-dimensional weak turbulence," Phys. Rev. E **86**, 036306 (2012).

[11] Y. Liao and N. T. Ouellette, "Spatial structure of spectral transport in two-dimensional flow," J. Fluid Mech. **725**, 281–298 (2013).

[12] D. H. Kelley and N. T. Ouellette, "Spatiotemporal persistence of spectral fluxes in two-dimensional weak turbulence," Phys. Fluids **23**, 115101 (2011).

[13] D. H. Kelley and N. T. Ouellette, "Separating stretching from folding in fluid mixing," Nat. Phys. **7**, 477–480 (2011).

[14] H. Xia, D. Byrne, G. Falkovich, and M. Shats, "Up-

scale energy transfer in thick turbulent fluid layers," Nat. Phys. **7**, 321–324 (2011).
[15] G. Boffetta and R. E. Ecke, "Two-dimensional turbulence," Annu. Rev. Fluid Mech. **44**, 427–451 (2012).
[16] D. H. Kelley and N. T. Ouellette, "Using particle tracking to measure flow instabilities in an undergraduate laboratory experiment," Am. J. Phys. **79**, 267–273 (2011).
[17] N. T. Ouellette, H. Xu, and E. Bodenschatz, "A quantitative study of three-dimensional Lagrangian particle tracking algorithms," Exp. Fluids **40**, 301–313 (2006).
[18] N. Mordant, A. M. Crawford, and E. Bodenschatz, "Experimental Lagrangian probability density function measurement," Physica D **193**, 245–251 (2004).
[19] S. B. Pope, *Turbulent Flows* (Cambridge University Press, Cambridge, 2000).
[20] M. Germano, "Turbulence: the filtering approach," J. Fluid Mech. **238**, 325–336 (1992).
[21] S. Liu, C. Meneveau, and J. Katz, "On the properties of similarity subgrid-scale models as deduced from measurements in a turbulent jet," J. Fluid Mech. **275**, 83–119 (1994).
[22] G. L. Eyink, "Local energy flux and the refined similarity hypothesis," J. Stat. Phys. **78**, 335–351 (1995).
[23] M. K. Rivera, W. B. Daniel, S. Y. Chen, and R. E. Ecke, "Energy and enstrophy transfer in decaying two-dimensional turbulence," Phys. Rev. Lett. **90**, 104502 (2003).
[24] S. Chen, R. E. Ecke, G. L. Eyink, X. Wang, and Z. Xiao, "Physical mechanism of the two-dimensional enstrophy cascade," Phys. Rev. Lett. **91**, 214501 (2003).
[25] S. Chen *et al.*, "Physical mechanism of the two-dimensional inverse energy cascade," Phys. Rev. Lett. **96**, 084502 (2006).
[26] Z. Xiao, M. Wan, S. Chen, and G. L. Eyink, "Physical mechanism the inverse energy cascade of two-dimensional turbulence: a numerical approach," J. Fluid Mech. **619**, 1–44 (2008).
[27] D. H. Kelley, M. R. Allshouse, and N. T. Ouellette, "Lagrangian coherent structures separate dynamically distinct regions in fluid flows," Phys. Rev. E **88**, 013017 (2013).
[28] R. Ni, G. A. Voth, and N. T. Ouellette, "Extracting turbulent spectral transfer from under-resolved velocity fields," Phys. Fluids **26**, 105017 (2014).
[29] R. H. Kraichnan, "Inertial ranges in two-dimensional turbulence," Phys. Fluids **10**, 1417–1423 (1967).
[30] C. E. Leith, "Diffusion approximation for two-dimensional turbulence," Phys. Fluids **11**, 671–673 (1967).
[31] G. K. Batchelor, "Computation of the energy spectrum in homogeneous two-dimensional turbulence," Phys. Fluids **12**, 11233–11239 (1969).
[32] E. Lindborg, "Comment on "Turbulence-condensate interaction in two dimensions"," Phys. Rev. Lett. **102**, 149401 (2009).
[33] P. M. Chaikin and T. C. Lubensky, *Principles of Condensed Matter Physics* (Cambridge University Press, Cambridge, 2000).
[34] H. Chaté, F. Ginelli, and R. Montagne, "Simple model for active nematics: quasi-long-range order and giant fluctuations," Phys. Rev. Lett. **96**, 180602 (2006).
[35] J. C. H. Fung and J. C. Vassilicos, "Two-particle dispersion in turbulentlike flows," Phys. Rev. E **57**, 1677–1690 (1998).
[36] E. Brown, A. Nikolaenko, and G. Ahlers, "Reorientation of the large-scale circulation in turbulent Rayleigh-Bénard convection," Phys. Rev. Lett. **95**, 084503 (2005).
[37] J. Sommeria, "Experimental study of the two-dimensional inverse energy cascade in a square box," J. Fluid Mech. **170**, 139–168 (1986).